Tsallis distributions of magnetic field strength variations in the heliosphere: 5 to 90 AU

L. F. Burlaga,[1] A. F-Viñas,[1] and C. Wang[2]

Received 1 March 2007; revised 15 March 2007; accepted 4 April 2007; published 7 July 2007.

[1] The Tsallis (q-exponential) distribution function, derived from the entropy principle of nonextensive statistical mechanics, describes fluctuations in the magnetic field strength on many scales throughout the heliosphere. This paper shows that a one-dimensional multifluid magnetohydrodynamic (MHD) model, with Advanced Composition Explorer (ACE) observations at 1 AU as input, predicts Tsallis distributions between 5 and 90 AU on scales from 1 to 128 days. At a scale of 1 day, the radial variation of the entropic index q decreases from $q \geq 5/3$ at $R \leq 50$ AU to $q \leq 5/3$ at $R \geq 60$ AU, corresponding to a change from a divergent to a convergent second moment of the Tsallis distribution, suggesting the possibility of a "phase transition" and/or a relaxation effect at $\approx$60 AU. The Tsallis distribution derived from the time series of one-dimensional MHD model is nearly identical to those observed by Voyager 1 at $\sim$80 AU over the scales from 1 to 64 days during the year 2000. The Tsallis distribution appears over a wide range of scales and distances despite the complex nonlinear dynamical evolution of the heliospheric magnetic field during 1999/2000.

Citation: Burlaga, L. F., A. F-Viñas, and C. Wang (2007), Tsallis distributions of magnetic field strength variations in the heliosphere: 5 to 90 AU, *J. Geophys. Res.*, *112*, A07206, doi:10.1029/2006JA012213.

1. Introduction

[2] Boltzmann-Gibbs statistical mechanics cannot describe nonequilibrium physical systems with large variability and multifractal structure such as the solar wind. Tsallis introduced a generalized statistical mechanics with an entropy function S_q describing the statistics and a constraint expressing the physics [*Tsallis*, 1988, 2004; *Tsallis and Brigatti*, 2004]. Choosing the nonextensive pseudoadditive entropy $S_q = \sum (p_i^q - 1)/(1 - q)$, ($p_i$ is the probability of the ith microstate, and q is a constant that measures the degree of nonextensivity) and extremizing S_q subject to two constraints, *Tsallis* [1988, 2004] derived the probability distribution (pdf)

$$y(x) = A\left[1 + (q-1) \times C \times x^2\right]^{-1/(q-1)} \tag{1}$$

where x is physical quantity such as energy and A, C, and q are constants at a given scale. In the limit $q \to 1$, the statistical mechanics of Tsallis reduces to that of Boltzmann and Gibbs, where the pdf is proportional to an exponential (Gaussian) distribution and x is energy. In the limit of large x, the Tsallis pdf (1) approaches the power law $D \times x^{-(2/(q-1))}$, where $D \equiv A[(q-1)C]^{-1/(q-1)}$.

[3] *Tsallis* [2004] notes that there are at least 20 entropy functions in the literature, and he compares several in detail. For example, *Rényi* [1970] introduced an extensive entropy, and *Daroczy* [1970] introduced "entropies of type B" related to Rényi entropies. These entropies are different than the Tsallis entropy. For example, the Rényi entropy is extensive, nonstable, and nonconcave; the Tsallis entropy is nonextensive, stable, and concave. Generalized statistics and power law distributions were discussed by many people, including *Hasegawa et al.* [1985] and *Kaniadakis* [2001]. It is possible to interpret the Tsallis distribution as a consequence of fluctuations, described by "superstatistics" [*Beck*, 2001, 2002a, 2002b, 2004; *Beck and Cohen*, 2003]. A statistical mechanical foundation for superstatistics was given by *Tsallis and Souza* [2003].

[4] The Tsallis distribution describes the probability density functions (pdfs) of fluctuations in increments of the magnetic field strength B in the solar wind at 1 AU on scales from 1 hour to 128 days near both solar maximum and minimum [*Burlaga and Viñas*, 2004a, 2005a]. The Tsallis distribution also describes fluctuations in the solar wind speed at 1 AU from scales of 64 s to 128 days [*Burlaga and Viñas*, 2004b]. *Leubner and Vörös* [2005a, 2005b] and *Vörös et al.* [2006] discuss distribution functions of small-scale intermittency and turbulence in the solar wind. Distribution functions associated with small-scale turbulence were discussed by *Arimitsu and Arimitsu* [2000, 2001a, 2001b, 2002a, 2002b, 2002c, 2002d, 2002e]. *Treumann et al.* [2004] discuss stationary states far from equilibrium for systems such as the solar wind. Tsallis distributions of large-scale fluctuations in the heliosheath were observed by *Burlaga et al.* [2006]. *Burlaga and Viñas* [2005b] found Tsallis distributions of daily observations of the fluctuation in B throughout each of the years 1980,

[1]NASA/Goddard Space Flight Center, Greenbelt, Maryland, USA.
[2]State Key Laboratory of Space Weather, Chinese Academy of Sciences, Beijing, China.

Copyright 2007 by the American Geophysical Union.
0148-0227/07/2006JA012213

1991, 2001, and 2002, when Voyager 1 (V1) was at 6.9–9.7, 43.6–47.2, 79.8–83.4, and 83.4–86.9 AU, respectively.

[5] The purpose of this paper is to show that Tsallis distributions of fluctuations in the increments of B between 5 and 90 AU on scales from 1 to 128 days and the parameters of these distributions are predicted by a deterministic one-dimensional time-dependent magnetohydrodynamic (MHD) model with Advanced Composition Explorer (ACE) observations at 1 AU as input. We also show that the predictions of the model agree with the observations from V1 at ~80 AU.

2. MHD Model and Magnetic Field Strength Profiles From 5 to 90 AU

[6] We use the numerical model of Chi Wang [*Wang and Richardson*, 2001a] (hereafter referred to as "the CW model"), which is a deterministic, one-dimensional, nonlinear multifluid, time-dependent MHD model that includes pickup protons and the neutral interstellar gas (with a neutral hydrogen density at the termination shock equal to 0.09/cc). The model is an extension of the model of *Isenberg* [1986]. The assumption of one dimension gives a good approximation for the nonlinear evolution of the principal features such as streams, shocks, and interaction regions [see, e.g., *Burlaga et al.*, 1985]. This MHD model has been used to successfully predict plasma and magnetic field observations at Voyager 2 (V2) of (among other things) (1) the evolution and interactions of ejecta and shocks; (2) the formation and evolution of global merged interaction regions ("GMIRs"); (3) the evolution of systems of corotating streams and corotating merged interaction regions; (4) The effects of the onset of fast flows in the declining phase of the solar cycle; (5) the statistical properties of ejecta at 5 AU; (6) unexpected correlations among speed density and magnetic field strength in the distant heliosphere; (7) the radial evolution of multiscale properties of the solar wind; (8) the multifractal structure of the heliospheric magnetic field; and (9) the radial evolution of the proton temperature [*Wang and Richardson*, 2001b, 2003; *Wang et al.*, 2001, 2003; *Richardson et al.*, 2003, 2006; *Burlaga et al.*, 2003a, 2003b, 2003c, 2005]. Of course, many other models have been developed to describe the solar wind (see, e. g., the reviews by *Burlaga* [1995], *Whang* [1991], and *Zank* [1999]), and it would be of interest to determine whether such models also predict Tsallis distributions of changes in B.

[7] We use hour averages of the ACE magnetic field $\mathbf{B}(t)$ and plasma data measured at 1 AU as input to the CW model, calculate daily averages of the magnetic field magnitude, $B(t)$, for approximately yearly intervals at distances of 5, 10, 15, 20, 30, 40, 50, 60, 70, 80, and 90 AU, and determine the pdfs of increments in $\mathbf{B}$ on scales between 1 and 128 days at each of these distances. The pdfs are fitted to the Tsallis distribution in order to ascertain whether the model can predict Tsallis distributions like those that have been observed. The use of hour averages, rather than higher resolution data, tends to smooth discontinuities and small-scale fluctuations; however, a one-dimensional MHD model with hour averages of the magnetic field and plasma as input can predict the evolution, formation, and merger of shocks and interaction regions, even between 1 and 2 AU [see, e.g., *Burlaga et al.*, 1985].

[8] The complexity that is predicted by the model is largely due to the variability introduced at 1 AU. We use hour averages of B, N, V and T as input conditions to the model in order to better capture the effects of (1) steep gradients in front of streams and elsewhere; (2) interaction regions, whose passage time is less than a day near 1 AU; (3) shocks and abrupt pressure changes; and (4) turbulence and waves. However, daily averages are computed beyond 1 AU in order to compare with the Voyager observations, which are incomplete on any given day owing to tracking limitations and the lack of on-board storage.

[9] The CW model with the ACE data for 1999 as input was used by *Burlaga et al.* [2003a] to describe both statistical properties of the solar wind and the formation, evolution, and decay of large-scale structures. The model predicts the development of merged interaction regions (MIRs) near 5–10 AU and a global merged interaction region ("GMIR") between 15 and 60 AU. A GMIR is a quasi-spherical shell of intense, structured magnetic fields that moves past a spacecraft over an interval of the order of 30–90 days, 1–3 solar rotations [*Burlaga et al.*, 1993; *Burlaga*, 1995; *McDonald and Burlaga*, 1997]. This paper extends the model results of *Burlaga et al.* [2003a] by presenting normalized magnetic field strength profiles (restricted to 256-day intervals), extending the profiles from 1 to 90 AU, and (most importantly) showing that the predicted multiscale distributions of the fluctuations in B can be described by the Tsallis distribution.

[10] The profiles of daily averages of $B/\langle B\rangle$ versus day (measured from 1 January 1999) are plotted in Figure 1; $\langle B\rangle$ is the average magnetic field strength over an interval of 1 year at the indicated distance. The plots are organized by increasing distance. The magnetic field data input to the model from ACE at 1 AU are shown in the top-left panel. The other panels show $B/\langle B\rangle$ versus time, predicted by the CW model. Large, quasiperiodic MIRs are present at 5 AU. The MIRs begin to damp out at 10 AU. A GMIR begins to develop at 15 AU. The GMIR grows in width and amplitude from 30 to 50 AU, then decays, and finally disappears by 80 AU.

3. Probability Distribution Functions of the Magnetic Field Strength Fluctuations

3.1. Introduction

[11] Section 3 presents the pdfs (histograms) of the fluctuations of B on scales between 1 and 128 days, derived from the profiles of $B/\langle B\rangle$ versus time computed from the CW model at various distances from the Sun between 5 and 90 AU. We show that all of the pdfs can be described accurately by the Tsallis distribution [equation (1)]. In particular, for a 256-day interval at each distance (centered at the maximum magnetic field in the GMIR and the corresponding regions in its precursor), we compute a set of pdfs (histograms) describing increments in relative magnetic field strength, $\mathrm{d}Bn(t_i) \equiv [B(t_i + \tau_n) - B(t_i)]/\langle B(t_i)\rangle$ on scales $\tau_n = 2^n$ days, where $n = 0, 1, 2, 3, 4, 5, 6$, and 7. Thus we consider fluctuations on scales from 1 to 128 days. These are "large-scale fluctuations," defined as those observed in a time series ≈1 yearlong for frequencies

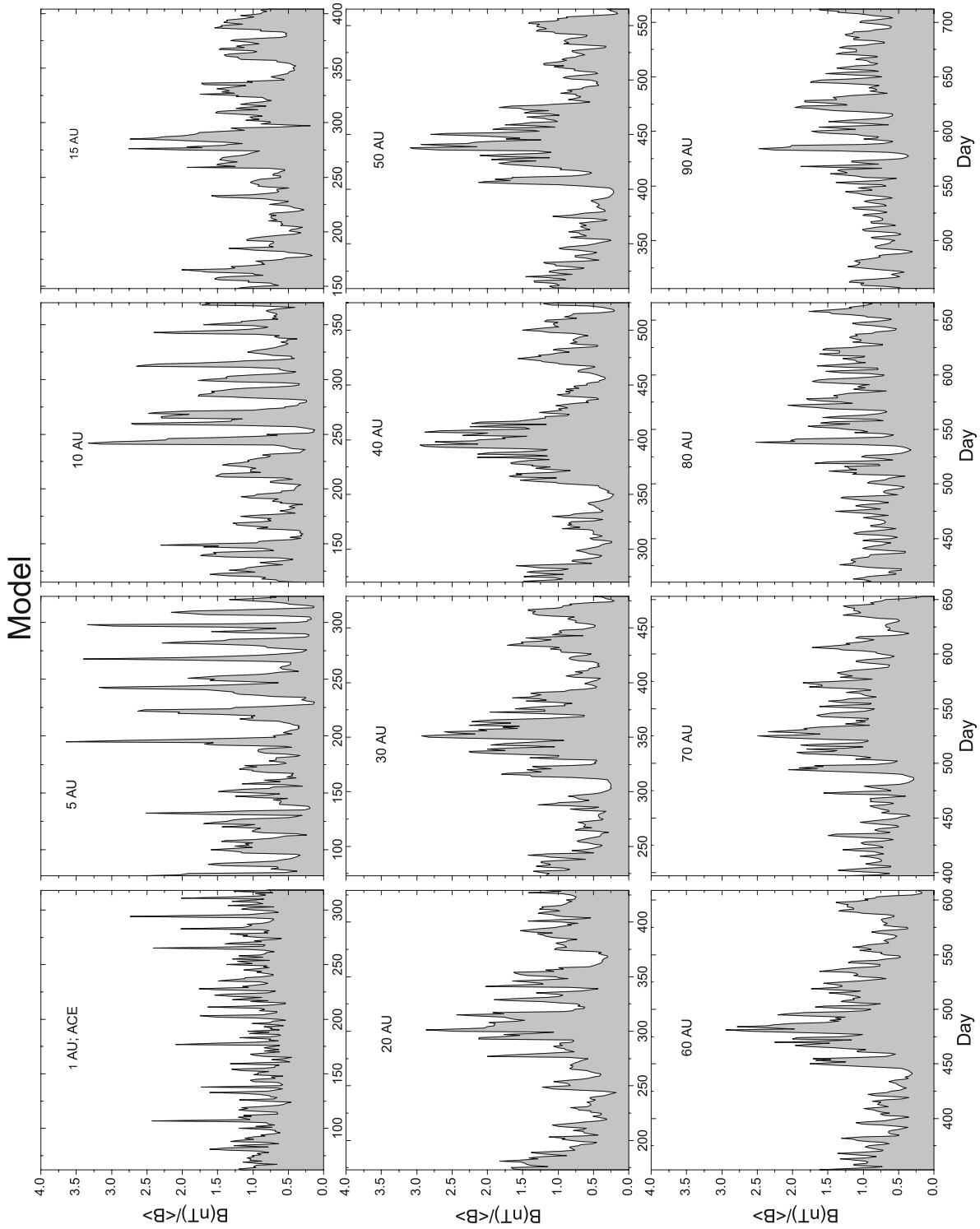

Figure 1. Top left: Daily averages of ACE observations of the magnetic-field strength at 1 AU during 1999 divided by the average magnetic field strength observed during 1999. Other panels: Computed profiles of daily averages of the normalized magnetic field strengths at 5, 10, 15, 20, 30, 40, 50, 60, 70, 80, and 90 AU showing the radial evolution of the profiles.

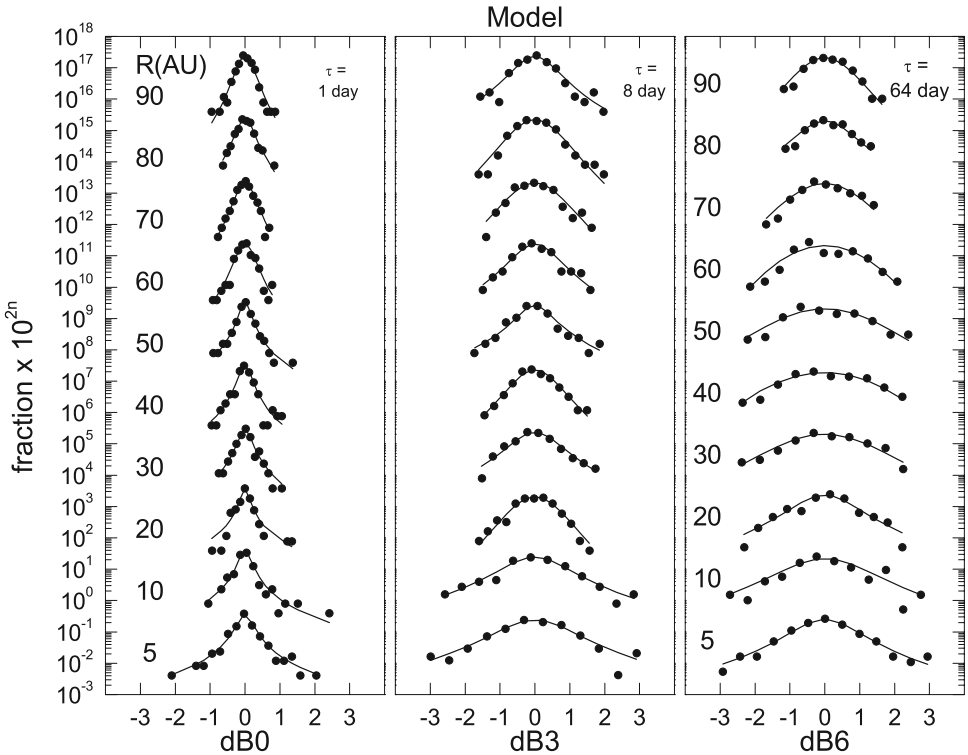

Figure 2. Left: Distributions of dB0 computed from time series predicted by the CW model at radial distances R from 5 to 90 AU (dots) and fits of the Tsallis distributions to the distributions of dB0. Middle: Distributions of dB3 computed from the CW model (dots) and fits of the Tsallis distributions (solid curves) to the distributions of dB3. Right: Distributions of dB3 computed from the CW model (dots) and fits of the Tsallis distributions (solid curves) to the distributions of dB3.

$\leq 3 \times 10^{-5}$ Hz, corresponding to a period of $\approx$10 hours [*Burlaga*, 1995]. The basic features of the radial evolution of dBn are revealed by pdfs of d$B0(R)$, d$B1(R)$ and d$B6$(R), corresponding to small (1 day), intermediate (8 days), and large scales (64 days). These results are plotted in Figures 2a, 2b, and 2c; each pdf is displaced a factor of 100 times above the one below it, for the sake of clarity. We fit the distributions of dBn derived from the time series predicted by the CW model to the Tsallis distribution (1) with $x^2 = (\mathrm{d}Bn)^2$, which is related to fluctuations in the magnetic energy density.

[12] Clearly, the parameters of the pdfs will depend on the interval considered. For example, the parameters for an interval that does not include the GMIR will differ from the parameters for an interval that does include the GMIR. When $q > 5/3$, the moments of the theoretical Tsallis pdfs diverge, and the parameters of the pdfs determined from a finite time series can depend on the length of the time series. Nevertheless, it is meaningful to compare the measured and predicted pdfs, if one considers intervals of the same length for the measured and predicted pdfs and intervals that contain the same types of features. We choose intervals of 256 days in both the observed and predicted time series, and we selected the portions of the predicted profile that are approximately centered about the GMIR.

[13] Since the size of the data set considered is limited (256 days), one should consider whether the results vary significantly when one changes the size of the data set and the width of the bins used in computing the pdfs. We performed a test for the stringent case $q > 5/3$ using the model predictions of d$B0$ for 30 AU. The result for pdf computed for a 256-day interval shown in Figure 2 is $q = 1.79 \pm 0.09$. Extending the interval to 376 days (the largest interval available) gives $q = 1.81 \pm 0.07$, so increasing the size of the interval does not significantly change the value of q relative to the quoted uncertainty $\pm$ 0.09. Increasing the bin size by a factor of 2 (decreasing the number of bins by a factor of 2) for the longer interval gives $q = 1.62 \pm 0.08$. The decrease in q is caused by smoothing the tail, to which q is very sensitive. Using smaller bins than chosen for the pdfs in Figure 2 would be desirable, but this is not possible because one arrives at 1 bin/count in parts of the tail even with the largest data set available in the solar wind. We conclude that the choice of the bin size and the quoted uncertainties of q are reasonable for the results of the model for 256-day intervals. The widths of the three distributions discussed above, measured by C, are the same within the quoted uncertainties, $C = 32 \pm 16$ for the 256-day interval in Figure 2; $C = 25 \pm 11$ (the 376-day interval); and $C = 39 \pm 18$ for the pdf computed with large bins.

3.2. Observed Distribution Functions and Fits With the Tsallis Distribution

[14] The solid curves in Figure 2 are fits of Tsallis distribution (2) to the distributions of d$Bn(R;\ \tau)$ derived from the CW model. The fits are obtained using the Levenberg-Marquardt algorithm [*Levenberg*, 1944; *Marquardt*, 1963; *Bard*, 1974] and a procedure discussed by *Burlaga and Viñas* [2004a, 2004b]. There is some scatter of the points in the tails of the distributions, where the counts

are low; the lowest number of counts in a bin is 0 or 1 in many cases. There are 256 points in the distributions for 1-day lags (τ = 1 day) and 128 points in the distributions for τ = 7. Despite the relatively small number of points, the quality of the fits measured by the correlation coefficient r is typically in the range from ≈0.92 to ≈0.99. We obtain the important result that the Tsallis distribution provides good fits to all of the pdfs predicted by the model, on all scales from 1 to 128 days and at all distances from 5 to 90 AU.

[15] The input to the CW model is a complex time series containing interaction regions, shocks, ejecta, and turbulence. The CW model predicts qualitative changes in the time series as the flow evolves with increasing distance. Shocks and interaction regions coalesce to form MIRs at 5–10 AU. A large GMIR begins to form at 15 AU, grows to a maximum size and amplitude at 40–50 AU, and then decays slowly. The growth of ordered large-scale structures with multifractal structures from chaotic combination of structures at 1 AU involves complex nonlinear interactions. Yet the complexity of the evolution is associated with a single pdf [equation (1)] for d$Bn(R; \tau)$.

[16] The shapes of the pdfs in Figure 2 reflect the shapes of the predicted profiles of $B/\langle B\rangle$ versus t in Figure 1. At a scale of 1 day, the pdfs of dB0 are relatively narrow at all distances, owing largely to the presence of small amplitude fluctuations. The tails of these pdfs (due in part to shocks and discontinuities) diminish with increasing R as the small-scale structures damp out and merge. Beyond 60 AU, these tails are less extended, becoming nearly parabolic (Gaussian) on a semilog scale. The core of the distributions is relatively narrow at all distances.

[17] At a scale of 8 days, the pdfs are very broad at 5 and 10 AU, with large tails corresponding to the large jumps associated with the MIRs and shocks predicted by the CW model (Figure 1). At larger distances, the width of the pdfs appears to be relatively uniform, although there are subtle variations in the shapes of the pdfs at various distances.

[18] Finally, at a scale of 64 days, the pdfs describe the largest structures. At 5 and 10 AU, the pdfs are broad and have large tails, corresponding to the MIRs in Figure 1. Between 20 and 70 AU, the shapes of the pdfs reflect the evolution of the GMIR. A pdf with a relatively narrow core and relatively small tails is observed at 20 AU, where the GMIR has begun to grow. At 30, 40, and 50 AU, where the GMIR with a complex internal structure is well developed, the core of the pdfs is broad, and the tails are not prominent. At 60 and 70 AU, where the GMIR is decaying, the cores of the pdfs become narrower. At 80 and 90 AU, where the GMIR has lost its identity, the pdfs are narrow and similar to one another.

[19] Since all of the pdfs in Figure 2 are described by the Tsallis distribution within the uncertainties of the fits, the multiscale evolution of the pdfs with increasing distance from the Sun can be described by the scale and distance dependence of the two functions $q(R; \tau)$ and $C(\tau)$.

3.3. Entropic Index q Versus Radial Distance

[20] The parameter q of the Tsallis distribution, the entropic index, is sensitive to both the core and the tails of the pdfs. We use the notation q_n to identify the value of q at the scale τ^n. Figure 2a shows q_n for n = 1, 3, and 6, as a function of distance R from the Sun, derived from the fits of the pdfs of dB0, dB3, and dB6, respectively from 5 to 90 AU (Figure 2).

[21] The variation of q_1 with R (Figure 3a) is described (nonuniquely) by a fit of the function $q_1 = A_2 + (A_1 - A_2)/(1 + \exp((R - R_o)/R_1))$ to the values of q_1 derived from fits of the Tsallis distributions to the observations in Figure 2. The quality of the fit is given by the coefficient of determination r^2 = 0.8. The function $q_1(R)$ asymptotically approaches A_1 = 2.07 ± 0.06 and A_2 = 1.44 ± 0.11 at small and large R, respectively. For values q_1 > 5/3 = 1.67, the theoretical second moment of the Tsallis distribution is infinite, and for q_1< 5/3, it is finite [see *Burlaga and Viñas*, 2005a and references therein]. The transition from divergent to convergent behavior occurs at $R_c \approx$ 58 AU (see Figure 3a), close to the inflection point R_o = 52 ± 6 AU of the sigmoid fit, which has a width R_1 = 11 ± 6 AU. This transition point is the distance at which the GMIR (Figure 1) begins to decay and the distance at which the width of the pdf of dB6 decreases (Figure 2). For $R \leq$ 40 AU, there are large jumps in $B(t)$ associated with the MIRs and the GMIR (Figure 1), giving large tails in the pdfs of dB0 (Figure 2a). For $R \geq$ 60 AU, the jumps in $B(t)$ diminish as the GMIR and fluctuations decay with increasing R (Figure 1), and there are no significant tails in the pdfs of dB0 (Figure 2a). At 60–90 AU, the large tails in the pdfs for dB0 are no longer present (q < 5/3), and the pdfs begin to approach a parabolic form indicative of an approach to Gaussian pdfs (q = 1) at the largest distances as the GMIR decays.

[22] The radial variation of q_3 for the pdfs of dB3 (τ = 8 days) and q_6 for the pdfs of dB6 (τ = 64 days) is shown by the closed circles and asterisks in Figures 3b and 3c, respectively. Three important results can be seen in Figure 3. First, the values of q_3 and q_6 for dB3 and dB6, respectively, versus R are all $\leq$ 5/3. Second, the values of q_6 for dB6 are closer to 1 (Gaussian) than the values of q_3 for dB3. Finally, the values of q_3 for dB3 tend to be intermediate between those for q_1 and q_6.

3.4. Width w of the Tsallis Distribution Function Versus Radial Distance

[23] The parameter $w \equiv 1/\sqrt{(C)}$ gives a measure of the width of the Tsallis distribution. Its behavior is similar to that of the standard deviation, but it has the advantage of being related to a parameter of the Tsallis distribution itself. Let w_n denote the value of w at the scale $\tau = 2^n$. The parameter w_n is shown as a function of R in Figure 4. The GMIR referred to above was discussed by *Burlaga et al.* [2003a] in the range 5–60 AU, in terms of the standard deviation of dBn, without reference to a physical pdf such as the Tsallis distribution. The GMIR is a large-scale structure, best seen in the pdfs of dB6 at a scale of 64 days. The width w_6 of the corresponding fluctuations in dB6, plotted in Figure 4, shows that the GMIR forms at ≈20 AU, grows to a maximum at ≈40 AU, and decays to the level of dB3 at 80–90 AU.

[24] Relatively large values of w_3 and w_8 for dB3 and dB8, respectively, are also observed at 5–10 AU. These are a manifestation of the MIRs in that region, as discussed by *Burlaga et al.* [2003a], who considered the standard deviation as a function of R and scale rather than w_n.

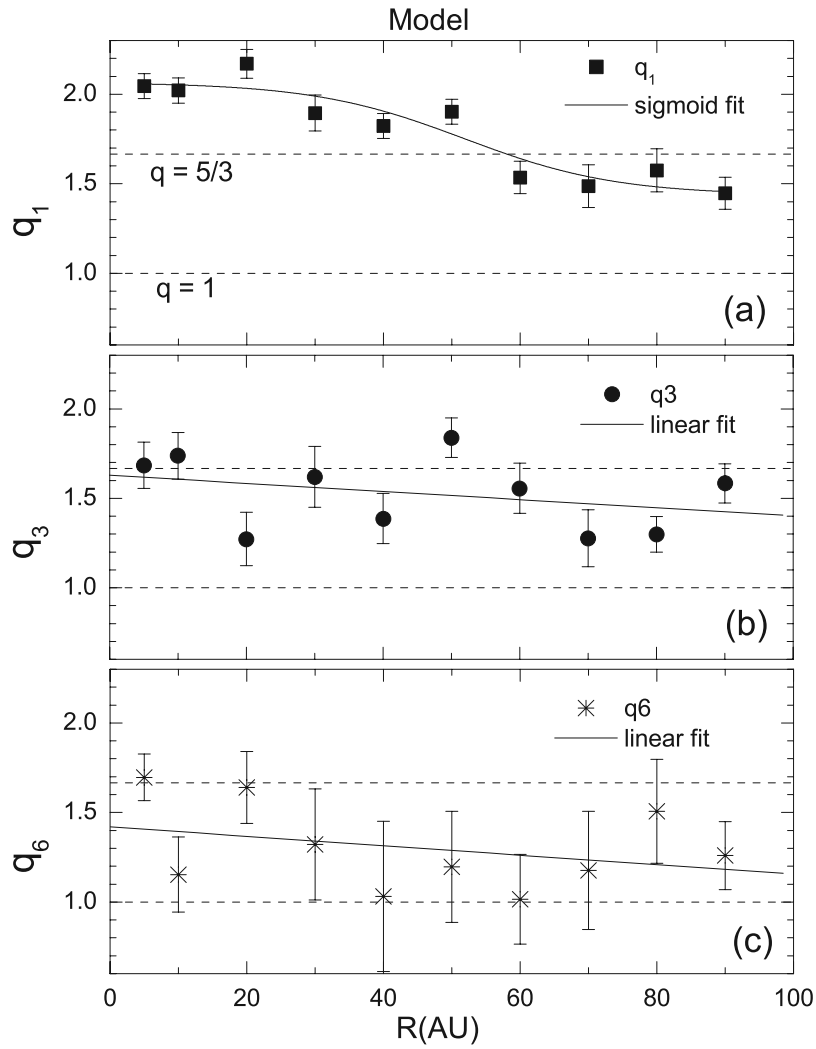

Figure 3. Top: The entropic index q_1 corresponding to a lag of 1 day (solid squares) and a fit of the sigmoid function (solid curve) as a function of radial distance R. Middle: The entropic index q_3 corresponding to a lag of 8 days (solid circles) and a linear fit (solid curve) as a function of radial distance R. Bottom: The entropic index q_8 corresponding to a lag of 64 days (asterisks) and a linear fit (solid curve) as a function of radial distance R.

[25] The fluctuations at the smallest scale $\tau = 1$ have relatively small amplitudes and consequently relatively narrow pdfs of dB0 at all distances. The widths w_1 are largest at 5 AU but rapidly decay as the small-scale fluctuations damp out and merge with increasing distance from the Sun. The width w_1 is nearly constant from 60 to 90 AU.

4. Comparison of the Multiscale Pdfs Predicted and Observed by V1

[26] V1 and V2 were making observations in the distant heliosphere during the year 2000 when they were in a position to sample the magnetic fields predicted from the model with the ACE data from 1999 as input.

[27] The GMIR predicted by the model (Figure 1) was observed by V2 near 60 AU [*Burlaga et al.*, 2003c], but the predicted internal structure is different than that observed. The V2 data have much larger uncertainties than the V1 data. Large amplitude quasiperiodic oscillations in B, with periods in the range $\approx$2–10 hours and beyond, are observed approximately half the time, probably originating in the V2 telemetry system. Twenty-five percent of the data have to be excluded for this reason. The resulting data gaps produce large artificial jumps in the data, giving spurious tails in the pdfs. An additional $\approx$25% of the data are also significantly contaminated. Finally, there is an uncertainty of $\approx$0.05 nT in each of the hour average measurements; this uncertainty is largely due to systematic errors which persist into the daily averages. This uncertainty tends to enhance the peak of the pdf for B between -0.5 and $+0.05$ nT. For these reasons, the pdfs observed by V2 do not agree with the predicted pdf at 60 AU. Since the discrepancy is largely a consequence of measurement uncertainties, we do not discuss the V2 observations further.

[28] The quality of the V1 data is much better than that of the V2 data. There are no "2- to 10-" hour oscillations, and the errors of the hour averages are $\approx\pm$0.02 nT. During the

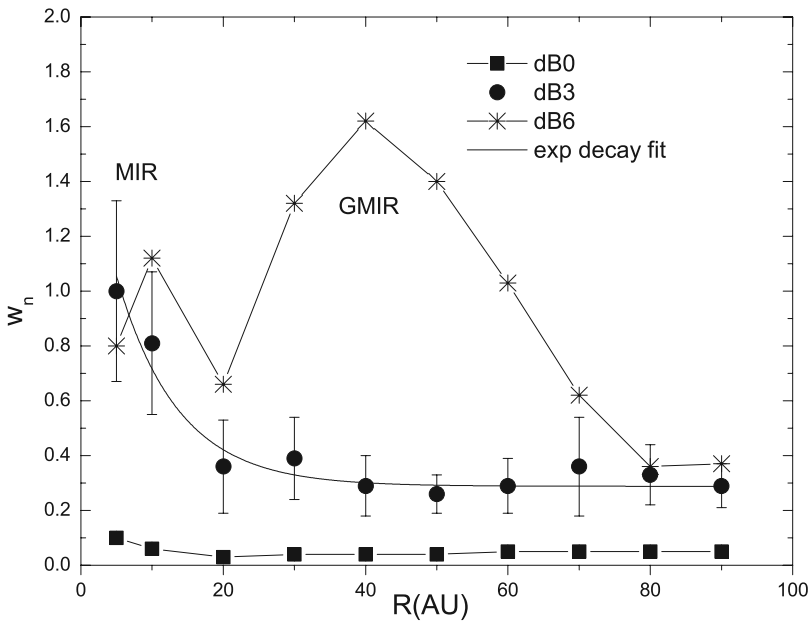

Figure 4. The width parameter w_n of the Tsallis distribution as a function of distance R, derived from fits to the predictions of the CW model for distributions of dB0, dB3, and dB6.

interval that we consider, from day of year (DOY) 68 to 324 of the year 2000, V1 moved from R = 76.81 to 79.34 AU and from latitude 33.6° to 33.7°N. The average speed measured by ACE at 1 AU during 1999 was 438 km/s, and the average speed at 80 AU predicted by the CW model is 346 km/s. Taking the mean speed between 1 and 80 AU to be the average of these numbers, ≈390 km/s, the time required for the solar wind to propagate from 1 to 78 AU at a mean speed of 390 km/s is 356 days. Thus during the year 2000, V1 was sampling the kinds of plasma and magnetic

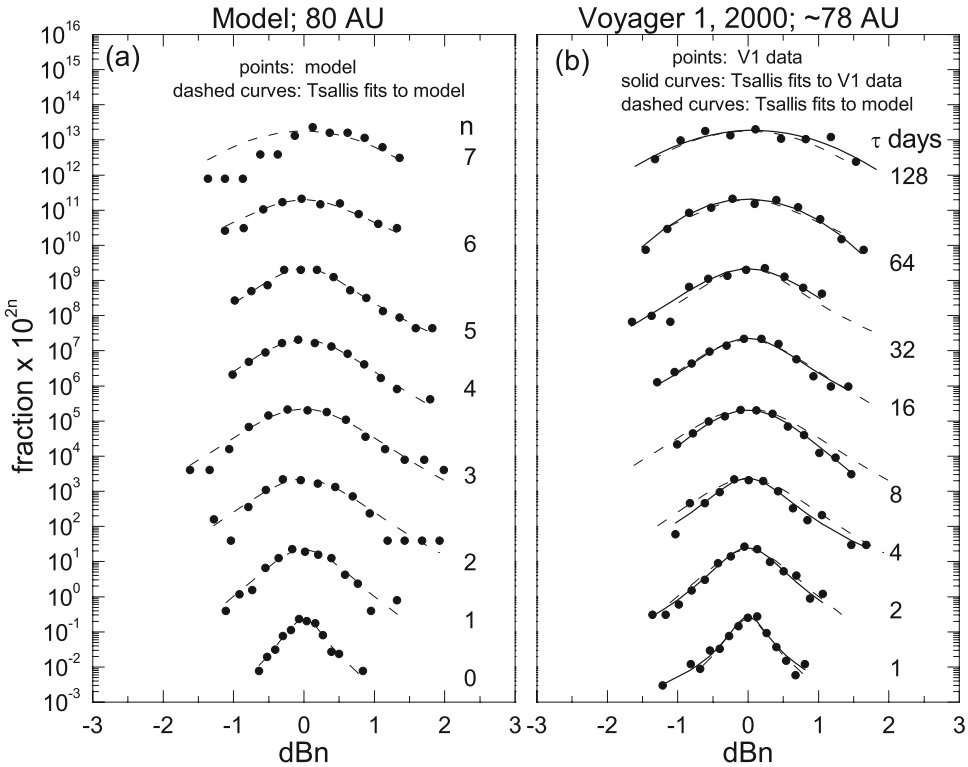

Figure 5. Left: Distributions of dBn on scales from 1 to 128 days computed from the CW model (filled circles) and fits of the Tsallis distribution to the predicted points (dashed curves). Right: Distributions of dBn on scales from 1 to 128 days derived from the Voyager 1 observations (filled circles); fits of the Tsallis distribution to the observed points (solid curves); and copies of the fits of the Tsallis distribution to the predicted points from the left panel (dashed curves).

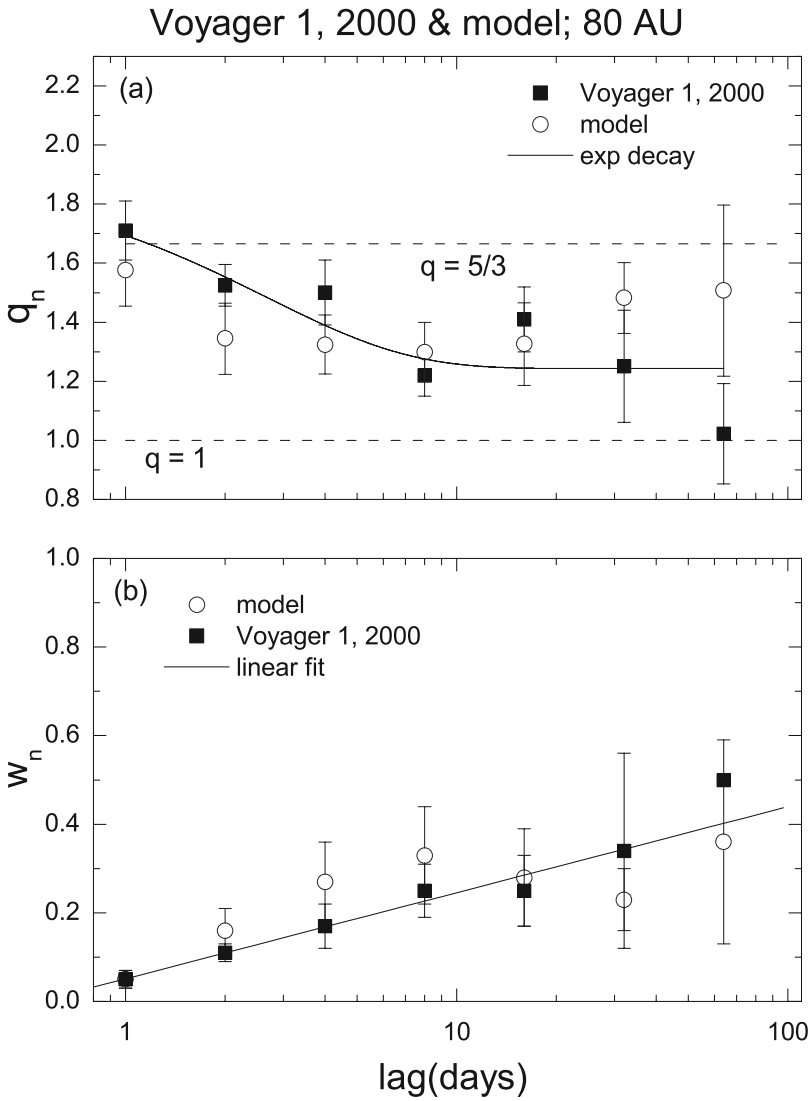

Figure 6. Top: The entropic index q_n derived from fits of the Tsallis distribution to the Voyager 1 observations of the distributions of d*B*n (filled squares) and the CW model (open circles) as a function of scale. The solid curve is a fit of the exponential decay curve to the q_n derived from Voyager 1 observations (filled squares). Bottom: The width parameter w_n derived from fits of the Tsallis distribution to the Voyager 1 observations of the distributions of d*B*n (filled squares) and the CW model (open circles) as a function of scale. The solid curve is a linear fit to the w_n derived from Voyager 1 observations.

fields that passed 1 AU during 1999, if the latitudinal variations are small. Of course, ACE and V1 were not radially aligned during this interval, since ACE moved around the Sun with Earth in the ecliptic, while V1 was relatively stationary at latitude 33.6°N. Nevertheless, *Burlaga et al.* [2003c] showed that the GMIR observed by V2 at ≈60 AU during the year 2000 was predicted by the CW model from the ACE observations, presumably because of the large size of the GMIR. One expects that the ACE observations provide a representative sample of the statistical fluctuations on a variety of scales at 1 AU during 1999. Accordingly, one might expect that the statistical properties of the magnetic field strength predicted at V1 are representative for that part of the solar cycle.

[29] The pdfs of d*Bn* for $n = 0, 1, 2, \ldots 7$, derived from the 256-day time series of $B/\langle B\rangle$ at 80 AU computed from the CW model, are shown by the closed circles in Figure 5a. The dashed curves show fits of the Tsallis distribution to these data. The pdfs derived from the CW model are described accurately by the Tsallis distribution on all scales, although the scatter of points increases at $\tau = 2^7 = 128$ days (where there are only 128 points in the time series) and in the extreme tails (where there are only 0 to a few points per bin). Thus the model predicts Tsallis distributions of d*Bn* on scales from 1 to 64 days at 80 AU.

[30] The pdfs of d*Bn* computed from the V1 data near 78 AU during 2000 in a 256-day interval containing the remnant of the GMIR are shown by the closed circles in Figure 5b for $n = 0$–7 ($\tau = 1$–128 days). Fits of the Tsallis distribution to these data are shown by the solid curves. The Tsallis distribution provides very good fits to the observed pdfs on all scales from 1 to 128 days.

[31] The dashed curves in Figure 5b are copies of the Tsallis fits to the pdfs derived from the CW model that are shown in Figure 5a, as discussed above. There is good agreement between the CW model and the observations. The Tsallis distributions derived from the time series of CW model at 80 AU are nearly identical to those observed by V1 on scales from 1 to 64 days.

[32] Figure 6a shows the values of q versus scale derived from fits of the Tsallis distribution to the V1 data together with those derived from fits of the Tsallis distributions obtained from the CW model time series at 80 AU. The predicted values of q agree with the observed values on all scales from 1 to 64 days within the uncertainties. Note that at 80 AU, $q \leq 5/3$ for all scales in Figure 6a. The points q versus τ derived from the V1 observations are described (non-uniquely) by an "exponential decay" $q = A \exp(-R/R_o) + y_o$, which shows a decrease from $q \approx 5/3$ at $\tau = 1$ to $q \approx 1.24 \pm 0.07$ at $8 \leq \tau \leq 64$ days, with a decay constant $R_o = 2.7 \pm 1.8$ days. The quality of the fit is measured by the coefficient of determination $r^2 = 0.78$. The results from the CW model are consistent with the V1 observations within the uncertainties.

[33] The widths of the pdfs observed and predicted at $\approx$80 AU are shown as a function of scale in Figure 6b. The width $w_n = 1/\sqrt{(C)}$ (obtained directly from the fits of the Tsallis distribution to the observed and predicted pdfs increases with increasing scale as shown in Figure 6b. The observed and predicted values of w_n are in agreement within the uncertainties.

5. Summary and Discussion

[34] The Tsallis distribution, derived from the entropy principle of nonextensive statistical mechanics, has been shown to describe fluctuations in the magnetic field strength on many scales throughout the heliosphere. This paper shows that a one-dimensional multifluid MHD model predicts the Tsallis distribution of dBn on a wide range of scales and distances during 1999/2000.

[35] We find that the Tsallis distribution of the nonextensive statistical mechanics of Tsallis describes the predicted probability distributions of increments of the magnetic field strength on scales from 1 to 128 days at distances between 5 and 90 AU. At a scale of 1 day, the variation of the parameters describing this distribution with scale reflect the change in character of the theoretical variance computed with the Tsallis distribution, from divergent ($q \geq 5/3$) at $R \leq 50$ AU to convergent ($q < 5/3$) at $R \geq 60$ AU. Between 5 and 50 AU, the magnetic field seems to be in a non-Gaussian state, even at large scales. However, beyond 60 AU, where the system has had time ($\approx$1 year) to relax and the system is close to a Gaussian equilibrium state at scales greater than the solar rotation period, it is still non-Gaussian at the smaller scales. The results suggest the possibility of a "phase transition" and/or a relaxation effect from $q > 5/3$ to $q < 5/3$ at $\approx$ 60 AU, as suggested by *Burlaga and Viñas* [2005b].

[36] V1 was located near 78 AU at latitude 33.6°N during the year 2000 in the interval that we consider (from DOY 68 to 324, 2000). Although ACE and V1 were not radially aligned during this interval, we have shown that it is possible to predict pdfs of large-scale fluctuations of the magnetic field strength on scales from 1 to 128 days observed by V1 from observations made at 1 AU by ACE, using a MHD model. We showed that the pdfs of the fluctuations observed by V1 could be fitted with the Tsallis distribution. The corresponding pdfs predicted at 80 AU are also Tsallis distributions. We showed that the predicted Tsallis distributions are nearly the same as the observed Tsallis distributions on scales from 1 to 64 days. The predicted values of entropic index q in the Tsallis distributions agree with the values observed by V1 on all scales from 1 to 64 days within the uncertainties, and we find that $q \leq 5/3$ for all scales. The entropic index decreases from $q \approx 1.6$ at a scale of $\tau = 1$ day to $q \approx 1.24 \pm 0.07$ at $8 \leq \tau \leq 64$ days. The widths of the pdfs observed and predicted on scales from 1 to 64 days are in agreement within the uncertainties.

[37] One should be able to describe the multiscale radial evolution of the observed multiscale Tsallis distributions as a solution of a suitable Fokker-Planck equation [*Anteneodo and Tsallis*, 2003; *Borland*, 1998; *Kaniadakis and Lapenta*, 2000; *Tsallis and Bukman*, 1996]. In this case, the evolution of the observed pdfs is viewed as an anomalous diffusion process in the presence of an additive and or multiplicative noise. This approach has it merits and should be pursued further. However, the CW model provides deeper physical insight into the dynamical origins of the evolution of the observed pdfs.

[38] **Acknowledgments.** The principal investigator of the magnetic field experiment on Voyager is N. F. Ness. We thank T. McClanahan and Sandy Kramer for their important contributions to the processing of the data used in this study. M. Acuña provided assistance evaluating the data. Chi Wang was supported by grant NNSFC 40325010.

[39] Wolfgang Baumjohann thanks Zoltan Voros and Manfred Leubner for their assistance in evaluating this paper.

References

Anteneodo, C., and C. Tsallis (2003), Multiplicative noise: A mechanism of leading to nonextensive statistical mechanics, *J. Math. Phys.*, *44*(11), 5194.

Arimitsu, T., and N. Arimitsu (2000), Tsallis statistics and fully developed turbulence, *J. Phys. A: Math. Gen.*, *33*, L235–L241.

Arimitsu, T., and N. Arimitsu (2001a), Analysis of turbulence by statistics based on generalized entropies, *Phys. A (Amsterdam)*, *295*(1–2), 177–194.

Arimitsu, T., and N. Arimitsu (2001b), Tsallis statistics and fully developed turbulence (vol 33 , pg L235, 2000), *J. Phys. A: Math. Gen.*, *34*(3), 673–674.

Arimitsu, N., and T. Arimitsu (2002a), Multifractal analysis of turbulence by using statistics based on non-extensive Tsallis' or extensive Renyi's entropy, *J. Korean Phys. Soc.*, *40*(6), 1032–1036.

Arimitsu, T., and N. Arimitsu (2002b), Analysis of velocity fluctuation in turbulence based on generalized statistics, *J. Phys.: Condens. Matter*, *14*(9), 2237–2246.

Arimitsu, T., and N. Arimitsu (2002c), PDF of velocity fluctuation in turbulence by a statistics based on generalized entropy, *Phys. A (Amsterdam)*, *305*(1–2), 218–226.

Arimitsu, T., and N. Arimitsu (2002d), Tsallis statistics and turbulence, *Chaos, Solitons Fractals*, *13*(3), 479–489.

Arimitsu, N., and T. Arimitsu (2002e), Analysis of velocity derivatives in turbulence based on generalized statistics, *Europhys. Lett.*, *60*(1), 60–65.

Bard, Y. (1974), *Nonlinear Parameter Estimation*, Chaps. 4–7, 54–216, Elsevier, New York.

Beck, C. (2001), On the small-scale statistics of Lagrangian turbulence, *Phys. Lett. A*, *287*, 240–244.

Beck, C. (2002a), Non-additivity of Tsallis entropies and fluctuations of temperature, *Europhys. Lett.*, *57*(3), 329–333.

Beck, C. (2002b), Generalized statistical mechanics and fully developed turbulence, *Phys. A (Amsterdam)*, *306*(1–4), 189–198.

Beck, C. (2004), Superstatistics: Theory and applications, *Continuum Mech. Thermodyn.*, *16*(3), 293–304.

Beck, C., and E. G. D. Cohen (2003), Superstatistics, *Phys. A (Amsterdam)*, *322*(1–4), 267–275.

Borland, L. (1998), Microscopic dynamics of the nonlinear Fokker-Planck equation: A phenomenological model, *Phys. Rev. E: Stat. Phys., Plasmas, Fluids, Relat. Interdiscip. Top.*, *57*(6), 6634.

Burlaga, L. F. (1995), *Interplanetary Magnetohydrodynamics,* Oxford Univ. Press, New York.

Burlaga, L. F., and A. F. Viñas (2004a), Multiscale structure of the magnetic field and speed at 1 AU during the declining phase of solar cycle 23 described by a generalized Tsallis probability distribution function, *J. Geophys. Res.*, *109*, A12107, doi:10.1029/2004JA010763.

Burlaga, L., and A. F. Viñas (2004b), Multi-scale probability distributions of solar wind speed fluctuations at 1 AU described by a generalized Tsallis distribution, *Geophys. Res. Lett.*, *31*, L16807, doi:10.1029/2004GL020715.

Burlaga, L., and A. F. Viñas (2005a), Triangle for the entropic index *q* of non-extensive statistical mechanics observed by Voyager 1 in the distant heliosphere, *Phys. A (Amsterdam)*, *356*(2–4), 375–384.

Burlaga, L., and A. F. Viñas (2005b), Tsallis distributions of the large-scale magnetic field strength fluctuations in the solar wind from 7 to 87 AU, *J. Geophys. Res.*, *110*, A07110, doi:10.1029/2005JA011132.

Burlaga, L. F., V. Pizzo, A. Lazarus, and P. Gazis (1985), Stream dynamics between 1 AU and 2 AU—A comparison of observations and theory, *J. Geophys. Res.*, *90*(A8), 7377–7388.

Burlaga, L. F., F. B. McDonald, and N.F. Ness (1993), Cosmic-ray modulation and the distant heliospheric magnetic field—Voyager-1 and Voyager-2 observations from 986 to 989, *J. Geophys. Res.*, *98*(A1), 1–11.

Burlaga, L. F., C. Wang, J. D. Richardson, and N. F. Ness (2003a), Large-scale magnetic field fluctuations and development of the 1999–2000 GMIR: 1 to 60 AU, *Astrophys. J.*, *585*(2), 1116–1158.

Burlaga, L. F., C. Wang, J. D. Richardson, and N. F. Ness (2003b), Evolution of magnetic fields in corotating interaction regions from 1 to 95 AU: Order to chaos, *Astrophys. J.*, *590*, 554.

Burlaga, L. F., N. F. Ness, F. B. McDonald, J. D. Richardson, and C. Wang (2003c), Voyagers 1 and 2 observations of magnetic fields and associated cosmic ray variations from 2000 through 2001; 60–87 AU, 549–549, *Astrophys. J.*, *582*, 540.

Burlaga, L. F., N. F. Ness, C. Wang, J. D. Richardson, F. B. McDonald, and E. C. Stone (2005), A transition to fast flows and its effects on the magnetic fields and cosmic rays observed by Voyager 2 near 70 AU, *Astrophys. J.*, *618*, 1074–1078.

Burlaga, L., A. Viñas, N. Ness, and M. H. Acuna (2006), Tsallis statistics of the magnetic field in the heliosheath, *Astrophys. J.*, *644*, L83–L86.

Daroczy, Z. (1970), Generalized information functions, *Inf. Control*, *16*(1), 36.

Hasegawa, A., K. Mima, and M. Duong-van (1985), Plasma distribution function in a superthermal radiation field, *Phys. Rev. Lett.*, *54*, 2608.

Isenberg, P. A. (1986), Interaction of the solar wind with interstellar neutral hydrogen: 3-Fluid model, *J. Geophys. Res.*, *91*(A9), 9965–9972.

Kaniadakis, G. (2001), Non-linear kinetics underlying generalized statistics, *Phys. A (Amsterdam)*, *296*(3–4), 405–425.

Kaniadakis, G., and G. Lapenta (2000), Microscopic dynamics underlying anomalous diffusion, *Phys. Rev. E: Stat. Phys., Plasmas, Fluids, Relat. Interdiscip. Top.*, *62*(3), 3246.

Leubner, M. P., and Z. Vörös (2005a), A nonextensive entropy path to probability distributions in solar wind turbulence, *Nonlinear Processes Geophys.*, *12*(2), 171–180.

Leubner, M. P., and Z. Vörös (2005b), A nonextensive entropy approach to solar wind intermittency, *Astrophys. J.*, *618*, 547–555.

Levenberg, K. (1944), A method for the solution of certain problems in least squares, *Q. Appl. Math.*, *2*, 164–168.

Marquardt, D. (1963), An algorithm for least-squares estimation of non-linear parameters, *SIAM J. Appl. Math.*, *11*, 431–441.

McDonald, F. B., and L. F. Burlaga (1997), Global merged interaction regions in the outer heliosphere, in *Cosmic Winds and the Heliosphere*, edited by J. R. Jokipii, C. P. Sonett, and M. S. Giampapa, 389–223.

Rényi, A. (1970), *Probability Theory*, Elsevier, New York.

Richardson, J. D., C. Whang, and L. Burlaga (2003), Correlated solar wind speed, density, and magnetic field changes at Voyager 2, *Geophys. Res. Lett.*, *30*(23), 2207, doi:10.1029/2003GL018253.

Richardson, J. D., Y. Liu, C. Wang, D. J. McComas, E.C. Stone, A. C. Cummings, L. F. Burlaga, and M. H. Acuna (2006), Source and consequences of a large shock near 79 AU, *Geophys. Res. Lett.*, *33*, L23107, doi:10.1029/2006GL027983.

Treumann, R. A., C. H. Jaroschek, and M. Scholer (2004), Stationary plasma states far from equilibrium, *Phys. Plasmas*, *11*(4), 1317–1325.

Tsallis, C. J. (1988), Possible generalization of Boltzmann-Gibbs statistics, *J. Stat. Phys.*, *52*, 479.

Tsallis, C. (2004), Nonextensive statistical mechanics: Construction and physical interpretation, in *Nonextensive Entropy-Interdisciplinary Applications*, edited by M. Gell-Mann and C. Tsallis, pp. 1–54, Oxford Univ. Press, New York.

Tsallis, C., and E. Brigatti (2004), Nonextensive statistical mechanics: A brief introduction, *Continuum Mech. Thermodyn.*, *16*, 223.

Tsallis, C., and D. Bukman (1996), Anomalous diffusion in the presence of external forces: Exact time-dependent solutions and their thermostatistical basis, *Phys. Rev. E: Stat. Phys., Plasmas, Fluids, Relat. Interdiscip. Top.*, *54*(3), R2197.

Tsallis, C., and M. C. Souza (2003), Constructing a statistical mechanics for Beck-Cohen superstatistics, *Phys. Rev. E: Stat. Phys., Plasmas, Fluids, Relat. Interdiscip. Top.*, *67*(026106), 1–5.

Vörös, Z., M. P. Leubner, and W. Baumjohann (2006), Cross-scale coupling-induced intermittency near interplanetary shocks, *J. Geophys. Res.*, *111*, A02102, doi:10.1029/2005JA011479.

Wang, C., and J. D. Richardson (2001a), Energy partition between solar wind protons and pickup ions in the distant heliosphere: A three-fluid approach, *J. Geophys. Res.*, *106*(A12), 29,401–29,407.

Wang, C., and J. D. Richardson (2001b), Voyager 2 observations of helium abundance enhancements from 1–60 AU, *J. Geophys. Res.*, *106*(A4), 5683–5692.

Wang, C., and J. D. Richardson (2003), Determination of the solar wind slowdown near solar maximum, *J. Geophys. Res.*, *108*(A2),1058, doi:10.1029/2002JA009322.

Wang, C., J. D. Richardson, and L. Burlaga (2001), Propagation of the Bastille Day 2000 CME shock in the outer heliosphere, *Sol. Phys.*, *204*(1–2), 411–421.

Wang, C., J. D. Richardson, L. F. Burlaga, and N. F. Ness (2003), On radial heliospheric magnetic fields: Voyager 2 observation and model, *J. Geophys. Res.*, *108*(A5), 1205, doi:10.1029/2002JA009809.

Whang, Y. C. (1991), Shock interactions in the outer heliosphere, *Space Sci. Rev.*, *57*(3–4), 339–388.

Zank, G. P. (1999), Interaction of the solar wind with the local interstellar medium: a theoretical perspective, *Space Sci. Rev.*, *89*(3–4), 413–688.

L. F. Burlaga and A. F-Viñas, NASA/Goddard Space Flight Center, Code 673, Greenbelt, MD 20771, USA. (leonard.f.burlaga@nasa.gov; adolfo.vinas@gsfc.nasa.gov)

C. Wang, State Key Laboratory of Space Weather, Chinese Academy of Sciences, Beijing, China. (cw@spaceweather.ac.cn)